DIRECT NUMERICAL SIMULATION AND LARGE-EDDY SIMULATIONS OF THE TURBULENT FLOW AROUND A NACA-0012 AIRFOIL

O. Lehmkuhl[*,†], A. Baez[*], I. Rodríguez[*] and C.D. Pérez-Segarra[*]

[*]Centre Tecnològic de Transferència de Calor (CTTC)
Universitat Politècnica de Catalunya (UPC)
ETSEIAT, Colom 11, 08222, Terrassa, Barcelona, Spain
Fax: +34 93 739 89 20 e-mail: cttc@cttc.upc.edu

[†]Termo Fluids, S.L.
Magí Colet, 8, 08204 Sabadell (Barcelona), Spain
e-mail: termofluids@termofluids.com

ABSTRACT

This paper investigates the capabilities of two subgrid-scale (SGS) models for predicting the complex flow in transitional separated bubbles. We consider here the flow over a NACA 0012 airfoil at Reynolds number $Re = 5 \times 10^4$ and angles of attack (AOA) $AOA = 5^\circ$ and 8°. The SGS models investigated are: the wall-adapting eddy viscosity model within a variational multiscale method (VMS-WALE) and the QR model. Both are well suited for LES in complex geometries with unstructured grids. The models are assessed and compared to the results of the direct numerical simulations (DNS) on the basis of first and second order statistics. Based on the good results obtained, a more challenging simulation is also performed at $Re = 1.44 \times 10^6$ and various AOA. It has been found that predictions of the lift and drag coefficients agree reasonably well with experimental data.

INTRODUCTION

The advances in computational fluid dynamics together with the increasing capacity of parallel computers have made possible to tackle complex turbulent problems by using high performance numerical techniques such as direct numerical simulation (DNS) and the development of modelling techniques such as Large-Eddy Simulation (LES) methods. DNS has a key role for improving the understanding of the turbulence phenomena and for the simulation of transitional flows in complex geometries, but it is still limited to low and moderate Reynolds numbers [1, 2, 3].

Considering the necessity of the use of LES models for studying engineering flows on complex geometries, which in general can not be described with structured grids, it is advisable to test models which do not use the wall-unit coordinates in their definition. In this sense, the Wall-Adapting Local-Eddy viscosity model [4] within the variational multiscale method [5] and the QR model [6] are two good recent choices which have been not sufficiently tested yet.

In the case of flow around airfoils, flow transition to turbulence undergoes in the initially laminar shear layer. After separation, at low AOA, the turbulent flow reattaches to the airfoil surface forming a bubble which directly affect the airfoil efficiency. The greater the separation bubble, the higher the loss of lift and the increase of drag. Thus, the study of the separation mechanism and the correct prediction of the location of boundary layer transition are both key aspects for improving engineering designs.

The aim of this work is to asses the performance of LES models for predicting the flow around a NACA 0012 airfoil with angle of attacks (AOA) of 5° and 8° at $Re = 5 \times 10^4$ based on the free-stream velocity (U_{ref}) and the chord length (C). To do so, first- and second-order statistics obtained with LES, carried out using the aforementioned subgrid-scale models (SGS) (VMS-WALE and QR models), are compared with the DNS results performed at both AOA. In addition, the performance of these models is studied in a more challenging situation at $Re = 1.44 \times 10^6$ and $AOA = 4^\circ, 8^\circ, 12^\circ, 14^\circ$ by comparison with experimental data.

MATHEMATICAL AND NUMERICAL MODEL

The Navier-Stokes and continuity equations can be written as

$$\mathsf{M}\boldsymbol{u} = \mathbf{0} \quad (1)$$

$$\frac{\partial \boldsymbol{u}}{\partial t} + \mathsf{C}(\boldsymbol{u})\,\boldsymbol{u} + \nu \mathsf{D}\boldsymbol{u} + \rho^{-1}\mathsf{G}\boldsymbol{p} = \mathbf{0} \quad (2)$$

where $\boldsymbol{u} \in \mathbb{R}^{3m}$ and $\boldsymbol{p} \in \mathbb{R}^{m}$ are the velocity vector and pressure, respectively (here m applies for the total number of control volumes (CV) of the discretised domain), ν is the kinematic viscosity and ρ the density. Convective and diffusive operators in the momentum equation for the velocity field are given by $\mathsf{C}(\boldsymbol{u}) = (\boldsymbol{u}\cdot\nabla) \in \mathbb{R}^{3m\times 3m}$, $\mathsf{D} = -\nabla^2 \in \mathbb{R}^{3m\times 3m}$ respectively. Gradient and divergence (of a vector) operators are given by $\mathsf{G} = \nabla \in \mathbb{R}^{3m\times m}$ and $\mathsf{M} = \nabla\cdot \in \mathbb{R}^{m\times 3m}$ respectively.

The governing equations have been discretised on a collocated unstructured grid arrangement by means of second-order spectro-consistent schemes [7]. Such schemes are conservative, i.e. they preserve the symmetry properties of the continuous differential operators and ensure both, stability and conservation of the kinetic-energy balance even at high Reynolds numbers and with coarse grids. For the temporal discretisation of the momentum equation (2) a two-steps linear explicit scheme on a fractional-step method has been used for the convective and diffusive terms, while for the pressure gradient term an implicit first-order scheme has been used. This methodology has been previously used with accurate results for solving the flow over bluff bodies with massive separation [8, 9].

The meshes used for solving the domain considered have been generated by a constant step extrusion of a two-dimensional (2D) unstructured grid. Under these conditions, the spanwise coupling of the discrete Poisson equation, which results from the incompressibility constrain, yields circulant sub-matrices that are diagonalizable in a Fourier space. This allows to solve the Poisson equation by means of a Fast Fourier Transform (FFT) method. The algorithm used is based on the explicit calculation and direct solution of a Schur Complement system for the independent 2D systems. For more details the reader is referred to [10].

By filtering the Navier-Stokes system of differential equations, SGS stress appears in the momentum equations which must be modelled in order to close the system. LES studies have been performed using two SGS models suitable for unstructured formulations: the QR model [6] and the wall-adapting local-eddy viscosity model within a variational multiscale formulation (VMS-WALE) [4, 5]. A brief description of these models is given hereafter.

QR-model: It was proposed by Verstappen [6] and is a SGS model based on the invariants of the rate-of-strain tensor which is proposed with the following advantages compared to the classical Smagorinsky formulation: i) $\nu_{sgs} = 0$ in any laminar flow, ii) $\nu_{sgs} = 0$ in any 2D flow, iii) $\nu_{sgs} \propto y^3$ near a wall and iv) $\nu_{sgs} \to 0$ when $l \propto Re^{\frac{-4}{3}}$. Further, it may be emphasized that the QR eddy-viscosity model is essentially not more complicated to implement in a LES-code than the standard Smagorinsky model (with c_s constant). Indeed, the QR-model is expressed in terms of the invariants of the rate-of-strain tensor and does not involve explicit filtering:

$$\begin{aligned}
\nu_{sgs} &= (c_{qr} l)^2 \frac{r^+}{q} \quad (3)\\
c_{qr} &= \frac{1}{\pi} + \frac{1}{24}\\
\overline{\mathcal{S}_{\mathsf{c}}} &= \frac{1}{2}[\mathsf{G}(\overline{\boldsymbol{u}_c}) + \mathsf{G}^*(\overline{\boldsymbol{u}_c})]\\
|\,\overline{\mathcal{S}_{\mathsf{c}}}\,| &= (2\overline{\mathcal{S}_{\mathsf{c}}\mathcal{S}_{\mathsf{c}}})^{1/2}\\
q &= \frac{1}{4}\,|\,\overline{\mathcal{S}_{\mathsf{c}}}\,|^2\\
r &= -det\overline{\mathcal{S}_{\mathsf{c}}}
\end{aligned}$$

WALE model within a variational multiscale framework: The variational multiscale (VMS) approach was originally formulated for the Smagorinsky model by Hughes [5] in the Fourier space, and is a promising approach for LES of turbulent flows. In VMS three classes of scales are considered: large, small and unresolved scales. If a second filter with filter length $\hat{l}$ is introduced (usually called test filter), a splitting of the scales can be performed,

$$f' = \overline{f} - \hat{f} \quad (4)$$

where following Vreman notation, f' is called the small-scale component, $\hat{f}$ the large-scale component and $\overline{f}$ is the original resolved quantity. Thus, for the

large-scale parts of the resolved $\overline{\boldsymbol{u}_c}$ a general governing equation can be derived,

$$\frac{\partial \overline{\boldsymbol{u}_c}}{\partial t} + \mathsf{C}\left(\overline{\boldsymbol{u}_c}\right)\overline{\boldsymbol{u}_c} + \nu \mathsf{D}\overline{\boldsymbol{u}_c} + \rho^{-1}\mathsf{G}\overline{\boldsymbol{p}_c} = -\frac{\partial \widehat{\mathcal{T}}_{\mathsf{c}}}{\partial x_j} - \frac{\partial \mathcal{T}_{\mathsf{c}}^{'}}{\partial x_j} \quad (5)$$

Inspecting Eqn. 5 it is possible to identificate $\widehat{\mathcal{T}}_{\mathsf{c}}$ as the subgrid term in the large-scale equation and $\mathcal{T}_{\mathsf{c}}^{'}$ as the subgrid small-scale term. Now, neglecting the effect of unresolved scales in the large-scale equation ($\widehat{\mathcal{T}}_{\mathsf{c}} \approx 0$) , we only need to model the $\mathcal{T}_{\mathsf{c}}^{'}$. In our implementation the *small-small* strategy is used in conjunction with the WALE model [4]:

$$\begin{aligned}
\mathcal{T}_{\mathsf{c}}^{'} &= -2\nu_s \mathcal{S}_{\mathsf{ij}}^{'} + \frac{1}{3}\mathcal{T}_{\mathsf{c}}^{'}\delta_{ij} \quad (6)\\
\nu_{sgs} &= (C_w^{vms}\Delta)^2 \frac{(\mathcal{V}_{\mathsf{ij}}^{'} : \mathcal{V}_{\mathsf{ij}}^{'})^{\frac{3}{2}}}{(\mathcal{S}_{\mathsf{ij}}^{'} : \mathcal{S}_{\mathsf{ij}}^{'})^{\frac{5}{2}} + (\mathcal{V}_{\mathsf{ij}}^{'} : \mathcal{V}_{\mathsf{ij}}^{'})^{\frac{5}{4}}}\\
\mathcal{S}_{\mathsf{ij}}^{'} &= \frac{1}{2}[\mathsf{G}(\overline{\boldsymbol{u}_c^{'}}) + \mathsf{G}^{*}(\overline{\boldsymbol{u}_c^{'}})]\\
\mathcal{V}_{\mathsf{ij}}^{'} &= \frac{1}{2}[\mathsf{G}(\overline{\boldsymbol{u}_c^{'}})^2 + \mathsf{G}^{*}(\overline{\boldsymbol{u}_c^{'}})^2] - \frac{1}{3}(\mathsf{G}(\overline{\boldsymbol{u}_c^{'}})^2\mathsf{I})
\end{aligned}$$

where C_w^{vms} is the equivalent of the WALE coefficient for the *small-small* VMS approach and in the finite volume context its value lies in the range between 0.3 and 0.5. In our studies a value of 0.325 is used.

PROBLEM DEFINITION AND COMPUTATIONAL DOMAIN

All computed flows are around a NACA-0012 airfoil extended to include sharp trailing edge. All coordinates are referred to body axes unless remarked. The x axis is chord-wise, y is in the plane of the airfoil and z is spanwise direction. Solutions are obtained in a computational domain of dimensions $40C \times 40C \times 0.2C$ with the leading edge of the airfoil placed at $(0, 0, 0)$ (see figure 1). Distances from the profile to the domain boundaries have been chosen according to previous experiences and potential vortices notions. The boundary conditions at the inflow consist of a uniform velocity profile (u,v,w)=$(U_{ref}\cos AOA,\ U_{ref}\sin AOA, 0)$. As for the outflow boundary, a pressure-based condition is imposed. No-slip conditions on the airfoil surface are prescribed. Periodic boundary conditions are used in the spanwise direction.

Figure 1: Computational domain. Blue boundary represents inflow conditions, with specified velocity and pressure. Red boundary represents outflow condition.

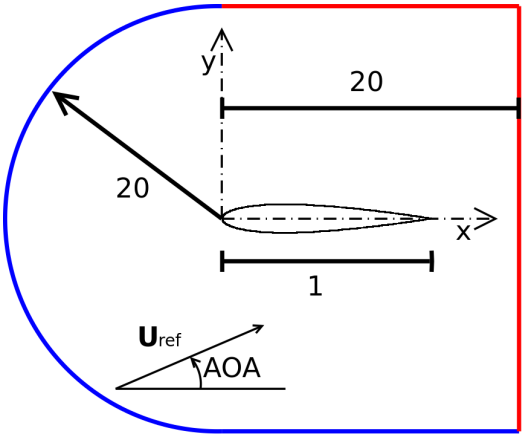

Flow around an airfoil at low AOA is mostly laminar with the exception of a zone close to the surface of the airfoil (suction side) and in the wake of it. In the turbulent zones the grid must be dense enough to capture all the flow scales. Within laminar zones, boundary layer must also be well-solved. Taking into account that the accuracy of the results in the region of the separated shear-layer where transition to turbulence occurs is highly grid dependent, care must be taken when the computational grid is constructed by clustering more control volumes in this zone. Another critical region is the near wake of the airfoil, where a poor grid resolution may cause notable upstream flow distortions. With these criteria, the governing equations are discretised on an unstructured mesh generated by the constant-step extrusion of a two-dimensional unstructured grid.

Table 1: Computational meshes. N_{2D} number of control volumes in the plane; N_{planes} number of planes in the spanwise direction; $NCVs$ total number of control volumes

Name	N_{2D}	N_{planes}	$NCVs \times 10^{-6}$
$LES-M1$	46417	16	0.74
$LES-M2$	149355	32	4.78
$DNS-5$	263522	96	25.3
$DNS-8$	280876	96	26.9

Grids used for LES and DNS are shown in the table 1. The presence of a laminar separation bubble (LSB) and detached shear-layer on the suction side makes

LES computations highly dependent on the mesh resolution. Hence, the behaviour of the two SGS models has been assessed on 2 different grids which have been constructed trying to set more resolution near the airfoil surface, while maintaining low the number of cells in the outer regions.

In *a-posteriori* analysis of the grid sizes used for DNS computations, the Kolmogorov length scale has been calculated. Table 2 shows the estimated Kolmogorov length scale and the actual grid-size used at different positions. For the $DNS-5$ mesh, the average value of this length scale has given $\eta/C = 1.74 \cdot 10^{-3}$ for the suction side region and about $\eta/C = 2.85 \cdot 10^{-3}$ in the near-wake ($1 \leqslant x/C \leqslant 2$). As is observed from the Table, the grid solved has an average size of $\overline{h}/C = 1.3 \cdot 10^{-3}$ in the suction side while in the near wake it is about $\overline{h}/C = 2.2 \cdot 10^{-3}$. For $DNS-8$ mesh, the average value of this length scale has given $\eta/C = 1.13 \cdot 10^{-3}$ for the suction side region and about $\eta/C = 1.65 \cdot 10^{-3}$ in the near-wake. Furthermore, the grid for the $AOA = 8°$ has an average size of $\overline{h}/C = 9.24 \cdot 10^{-4}$ in the suction side while in the near wake it is about $\overline{h}/C = 1.53 \cdot 10^{-3}$. With these ratios between grid-size and Kolmogorov scale, the grid density obtained for both meshes should be fine enough for solving the smallest flow scales in the suction side of the airfoil and in the near wake.

Table 2: Characteristic sizes of the meshes used for DNS at Re 5×10^4. Left: $AOA = 5°$ Right: $AOA = 8°$. $h = (\Delta_{2D}^2 \times \Delta_z)^{1/3}$ being Δ_{2D} the characteristic length in the 2D plane and Δ_z CV length in the spanwise direction.

$DNS-5$			$DNS-8$		
x	y	h/η	x	y	$\overline{h}/\eta$
0.40	0.063	0.87	0.15	0.057	0.90
0.60	0.058	1.10	0.30	0.083	2.61
0.80	0.040	0.59	0.30	0.066	1.40
0.80	0.100	0.26	0.60	0.066	0.63
0.95	0.020	0.61	0.80	0.066	0.61
1.05	0.000	0.82	0.95	0.025	0.54
1.20	0.100	0.38	1.05	0.000	1.34
2.00	0.000	0.78	1.20	0.070	0.87

RESULTS

For obtaining the numerical results presented, simulations have been advanced in time until statistical stationary flow conditions have been achieved. Once the initial transient has been washed out, results have been obtained based on the integration of instantaneous data over a sufficiently long-time period. It has been found, that the dynamics of the laminar separation bubble (LSB), even at the low $AOA = 5°$ is dominated by a low-frequency (f_m) with a time scale much larger than of the vortex shedding frequency. As a consequence, in order to well capture this phenomena, time integration has been fixed to 210 vortex-shedding periods for DNS simulations, while for LES computations it has been about 600 vortex-shedding periods.

DNS results: Instantaneous spanwise vorticity contours of the flow in the separated region for the two AOA under study are depicted in figure 2. As can be seen from the figure, at both AOA, the flow separates laminarly from the leading edge of the airfoil. Flow separation occurs as a consequence of the adverse pressure gradient on the suction side of the airfoil which leads to the formation of a LSB. Due to the strong pressure gradient, disturbances in the laminar separated shear-layer get amplified triggering the transition to turbulence.

Figure 3 shows the mean pressure coefficient, C_p, of the airfoil for both AOA obtained from DNS data. As the AOA increases, the adverse pressure-gradient increases and the flow is decelerated, which results in a movement of the laminar separation point toward the leading-edge increasing the height of the separated bubble, while at the same time, the turbulent separated region moves forward from the trailing edge. The plateau observed in the pressure distribution is a characteristic of the LSB. Transition to turbulence also occurs within a shorter distance. Due to the increase in the turbulent shear stress after transition, the flow reattaches to the airfoil surface with the decrease in the pressure coefficient after reattachment. In the figures 2 and 3 can also be observed, that with the increase in the AOA the bubble length decreases.

This can be also observed in the profiles of the turbulent shear stresses and turbulent kinetic energy from our simulations (not shown here). The turbulent shear stress, which causes transport of momentum in the boundary layer, is also responsible for the closure of the laminar separation bubble. The high values of turbulent shear stresses and turbulent kinetic energy in the region near the reattachment are strongly related with the vortex breakdown and turbulent transport.

Figure 2: Instantaneous spanwise vorticity contours of the flow around a NACA 0012 at $Re = 5 \cdot 10^5$. (top) $AOA = 5°$ and (bottom) $AOA = 8°$.

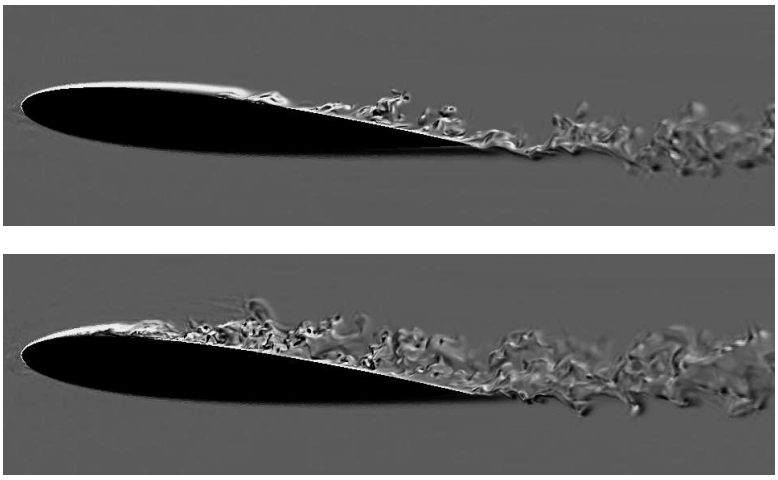

Figure 3: Results from DNS simulations. Pressure coefficient distribution for both AOA

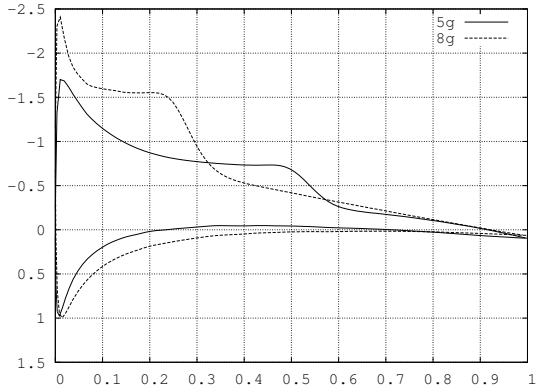

LES results: In table 3 the main flow characteristics obtained with both models are compared with DNS results. Both models predicts drag and lift coefficients with reasonable agreement even with the coarse grid. However the length of the recirculation bubble is better predicted with VMS-WALE model than with QR model.

In figures 4 and 5 a comparison of the streamwise velocity profiles and Reynolds stresses at different positions of the airfoil surface and wake are plotted for both models for $AOA = 8°$. The detailed comparison of the local data allows to evaluate how both SGS models are performing. Although both models approach to DNS results, it is observed that VMS-WALE model presents a better trend as the mesh is refined. This is specially true for the higher AOA. This case is more challenging with a largest vortex breakdown region and higher turbulence intensities. Largest differences are observed in the transitional region, as both models overpredict the reattachment location.

Table 3: Aerodynamic coefficients for the DNS and LES cases. $Re = 5 \cdot 10^4$.

Case	c_L	c_D	x_{sep}	x_{reat}
		$AOA = 5°$		
DNS	0.569	0.0291	0.0645	0.566
VMS-LES-M1	0.582	0.0248	0.140	0.571
VMS-LES-M2	0.561	0.0242	0.117	0.548
QR-LES-M1	0.586	0.0369	0.156	0.700
QR-LES-M2	0.565	0.0252	0.117	0.607
		$AOA = 8°$		
DNS	0.759	0.0497	0.0241	0.320
VMS-LES-M1	0.784	0.0536	0.0847	0.392
VMS-LES-M2	0.750	0.0460	0.0546	0.386
QR-LES-M1	0.805	0.0510	0.119	0.490
QR-LES-M2	0.760	0.0517	0.0833	0.418

Considering both, the integral quantities of table 3 and the local profiles of figure 5, QR model is less accurate than VMS-WALE with the coarser mesh. This behaviour may be related to an excessive dissipation at the large scales of the flow. This dissipation is always present but it is more apparent on coarser meshes. On the other hand, the scale separation of the VMS methodology prevents the model to alter the larger scales of the flow, allowing the VMS-WALE to predict quite accurate the general behavior of the flow even with very coarse meshes. However, as the mesh

is refined both models yield similar results.

Yet, LES results present largest differences on the prediction of the LSB size. Thus, a better mesh refinement strategy have to be done at this zone, since all the models give $\nu_{sgs} = 0$ in the LSB area. Analyzing DNS meshes it is very clear that for the laminar zone of the flow, a quasi DNS mesh is needed. On the other hand, after the reattachment, LES models capture well all the turbulent features of the flow without problems. Thus, in future works, a local refinement strategy in order to reduce the errors of the reattachment location will we used, increasing the spacial resolution only in the laminar zones of the flow.

Figure 4: LES results obtained with VMS-WALE model. Comparison with DNS data at $AOA = 8°$ at different positions of the airfoil surface and wake.

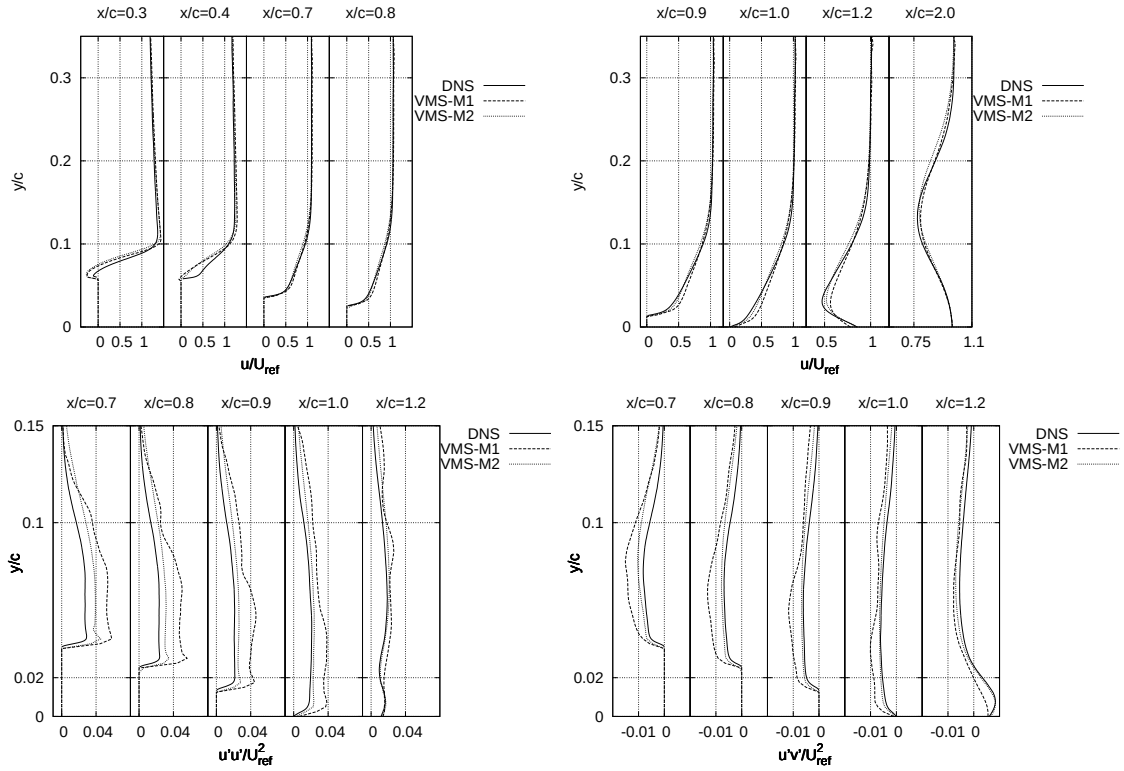

Figure 5: LES results obtained with QR model. Comparison with DNS data at $AOA = 8°$ at different positions of the airfoil surface and wake.

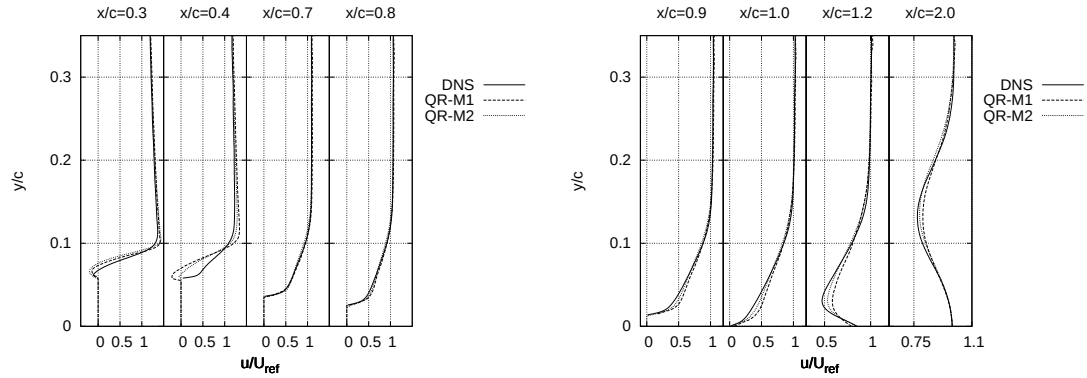

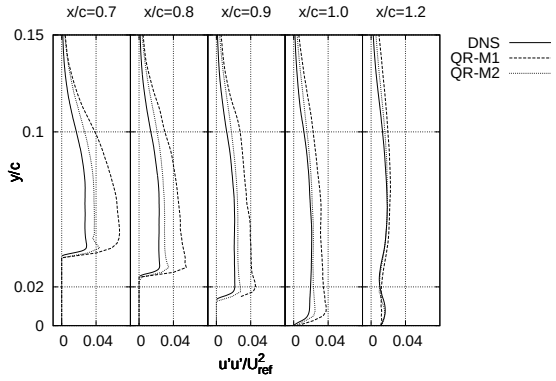

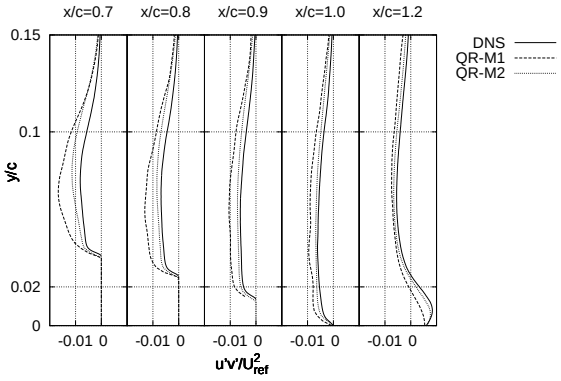

Figure 7: Drag coefficient at different AOA. Comparison with experimental data from different sources

Challenging LES: Stall on airfoils is caused by massive separation of the flow leading to a sharp drop in the lift and an increase in the drag over the airfoil surface. NACA 0012 airfoil exhibits two types of stall. A trailing-edge stall at all Reynolds numbers and a combined leading-edge/trailing-edge stall at intermediate Reynolds number. The latter shows the combined presence at stall of a turbulent boundary layer separation moving forward from the trailing-edge and a small laminar bubble in the leading-edge region failing to reattach which complete the flow breakdown. Thus, it is of interest to test the capability of LES models to deal with these complex physics.

Figure 6: Lift coefficient at different AOA. Comparison with experimental data from different sources

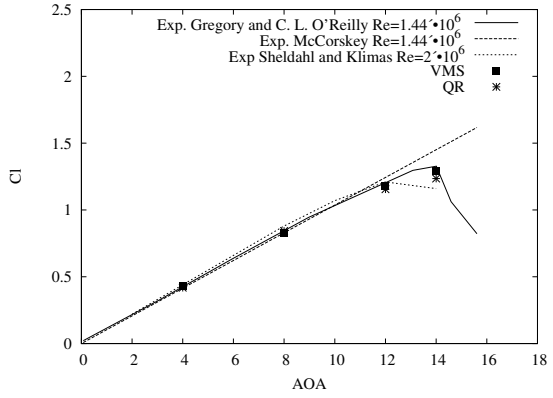

The selected Reynolds number to asses the performance of LES models is $Re = 1.44 \times 10^6$ with $AOA = 4°, 8°, 12°, 14°$. Similar to the previous section, the three-dimensional (3D) physical domain of the simulation consist of $40C \times 40C \times 0.2C$ with the airfoil at its center. Simulations have been performed on unstructured grids of 149355×32 planes. Notice that the same mesh have been used for all the different AOA.

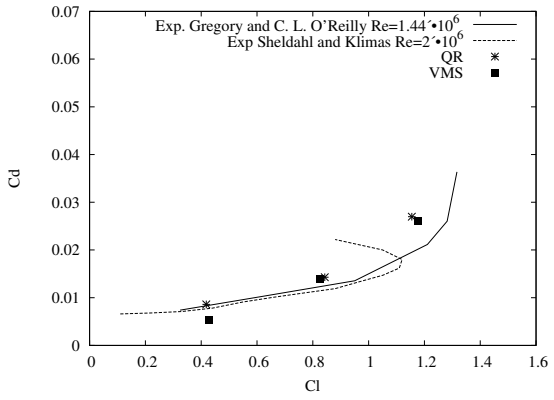

LES results have been compared with correlated experimental data which was obtained in more than 40 wind tunnels [11]. However, these correlations are not suitable when laminar separation bubble are presented in the profile. Thus, for these cases experimental data from Gregory and C. L. O'Reilly at $Re = 1.44 \cdot 10^6$ [12] and Sheldahl and Klimas at $Re = 2 \cdot 10^6$ [13] will be used in the assessment of the models.

Lift and drag coefficients at different AOA obtained with both models are depicted in figures 6 and 7. These results are quite satisfactory considering the grids used. For the higher AOA, errors in the drag coefficient prediction are the largest, as near stall and in stall massive separation occur and finer grids would be required. The influence of grid refinement into drag coefficient will be investigated in the future, considering local refinement in the leading-edge region for predicting well the laminar separation bubble that appears near this zone of the airfoil during stall.

CONCLUSIONS

Numerical simulations of the flow over a NACA 0012 airfoil at $Re = 5 \times 10^4$ and angles of attack of $AOA = 5°, 8°$ have been performed. Both cases exhibit laminar separation and transition to turbulence in the separated shear-layer.

A second-order spectro-consistent scheme for collocated and unstructured grids has been used in the discretisation of the governing equations. The conservation properties ensure good stability and conservation of the kinetic-energy balance with coarse meshes even at high Reynolds numbers. All the results have been computed on unstructured grids generated by the constant-step extrusion of a two-dimensional unstructured grid. For solving the Poisson equation, which arises from the incompressibility constrain a Fourier diagonalization method which takes advantage of the homogeneity of our discretisation in the spanwise direction has been used. The methodology developed for solving bluff bodies using unstructured grids has allowed to accurately solve the flow with very good results.

The performance of two subgrid-scale models, the wall-adapting local-eddy viscosity model within the variational multiscale method (VMS-WALE) and the QR model have been assessed by means of the direct comparison with DNS data. Both models performs quite well being capable of predicting separation and transition to turbulence, as well as the fully developed turbulence in the wake. In addition, a more challenging case for LES models at a higher Reynolds number of $Re = 1.44 \times 10^6$ and different AOA has been also carried out. Lift coefficient is predicted within an acceptable error considering the grids used. For the higher AOA, errors in the drag coefficient prediction are the largest, as near stall and in stall massive separation occur and finer grids would be required. The influence of grid refinement into drag coefficient will be investigated in the future, considering finer grids for predicting well the laminar separation bubble that appears near the leading-edge of the airfoil during stall.

ACKNOWLEDGEMENTS

This work has been by financially supported by the Ministerio de Educación y Ciencia, Secretaría de Estado de Universidades e Investigación, Spain (ref. ENE2009-07689) and by the Collaboration Project between Universidad Politècnica de Catalunya and Termo Fluids S.L. (ref. C06650)

REFERENCES

[1] Y. Hoarau, D. Faghani, M. Braza, R. Perrin, Anne-Archard, and Ruiz. *Flow, Turbulence and Combustion*, 71:119–132, 2003.

[2] H. Shan, L. Jiang, and C. Liu. *Computers & Fluids*, 34(9):1096–1114, 2005.

[3] L.E. Jones, R.D. Sandberg, and N.D. Sandham. *Journal of Fluid Mechanics*, 602:175–207, 2008.

[4] F. Nicoud and F. Ducros. *Flow, Turbulence and Combustion*, 62:183–200, 1999.

[5] T.J.R. Hughes, L. Mazzei, and K.E. Jansen. *Computing and Visualization in Science*, 3:47–59, 2000.

[6] R. Verstappen. In ERCOFTAC Series, editor, *Quality and Reliability of Large-Eddy Simulations II*, volume 16, pages 421–430, 2011.

[7] R. W. C. P. Verstappen and A. E. P. Veldman. *Journal of Computational Physics*, 187:343–368, May 2003.

[8] O. Lehmkuhl and R. Borrell and J. Chivas and C.D. Perez-Segarra In THMT09 *Turbulence Heat and Mass Transfer*, Rome, 2009.

[9] I. Rodriguez, R. Borrell, O. Lehmkuhl, C.D. Perez-Segarra and A. Oliva. *Journal of Fluid Mechanics*, In Press, 2011

[10] R. Borrell, O. Lehmkuhl, F.X. Trias, and A. Oliva. *Journal of Computational Physics*, In Press, Corrected Proof:–, 2011

[11] W.J. McCroskey. Technical report, National Aeronautics and Space Administration, 1987.

[12] N. Gregory and C.L. O'Reilly. Technical report, Ministry of Defence. Aeronautical Research council, London, 1973.

[13] R.E. Sheldahl and P.C. Klimas. Technical report, Sandia National laboratories, 1980.